ACS APPLIED MATERIALS & INTERFACES

Research Article

www.acsami.org

Optical Microring Resonators Constructed from Organic Dye Nanofibers and Their Application to Miniaturized Channel Drop/Add Filters

Ken Takazawa,* Jun-ichi Inoue, and Kazutaka Mitsuishi

National Institute for Materials Science, 3-13 Sakura, Tsukuba, 305-0003, Japan

ABSTRACT: We fabricated micrometer-scale optical ring resonators by micromanipulation of thiacyanine (TC) dye nanofibers that propagate exciton polaritons (EPs) along the fiber axis. High mechanical flexibility of the nanofibers and a low bending loss property of EP propagation enabled the fabrication of microring resonators with an average radius (r_{ave}) as small as 1.6 μm. The performances of the fabricated resonators (r_{ave} = 1.6−8.9 μm) were investigated by spatially resolved microscopy techniques. The Q-factors and finesses were evaluated as $Q \approx 300-3500$ and $F \approx 2-12$. On the basis of the r_{ave}-dependence of resonator performances, we revealed the origin of losses in the resonators. To demonstrate the applicability of the microring resonators to photonic devices, we fabricated a channel drop filter that comprises a ring resonator (r_{ave} = 3.9 μm) and an I/O bus channel nanofiber. The device exhibited high extinction ratios (4−6 dB) for its micrometer-scale dimensions. Moreover, we successfully fabricated a channel add filter comprising a ring resonator (r_{ave} = 4.3 μm) and two I/O bus channel nanofibers. Our results demonstrated a remarkable potential for the application of TC nanofibers to miniaturized photonic circuit devices.

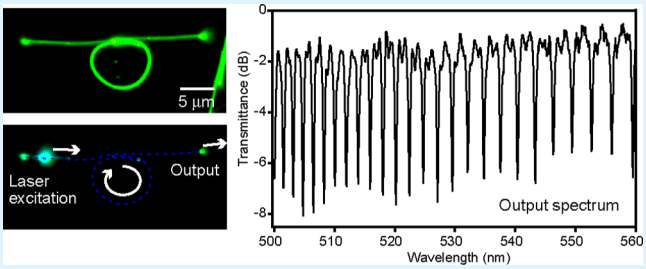

KEYWORDS: *photonics, nanofiber, organic dye, micromanipulation, ring resonator*

1. INTRODUCTION

Subwavelength waveguides that allow manipulation of optical signals at the nanometer to micrometer scale are essential building blocks in miniaturized photonic circuits, which have promising applications in various fields such as telecommunication and computing.[1] Therefore, photonic crystal waveguides,[2,3] plasmon waveguides,[4,5] silicon on insulator waveguides,[6,7] and semiconductor nanowires[8,9] have been extensively developed. Promising new candidates that are currently attracting considerable interest for subwavelength waveguides include self-assembled nanofibers of organic molecules. It has been observed that these nanofibers function both as active waveguides, which propagate their fluorescence (FL) generated by laser excitation along the fiber axis[10−23] and as passive waveguides, which directly propagate input laser light.[24−26] A nanofiber of thiacyanine dye (TC, Figure 1a) self-assembled in a solution is one of such nanofibers that serves as an efficient active waveguide.[10,27] Panels b and c in Figure 1 show an optical micrograph and FL microscopy image, respectively, of an ∼200 nm wide and ∼40 μm long TC nanofiber, which was transferred from a solution onto a glass substrate. When the nanofiber was illuminated with a focused laser beam with a wavelength within the exciton absorption band, FL spots were observed at both tips as well as the excitation position, showing that the nanofiber indeed behaves as an active waveguide (Figure 1d). The fact that no FL was observed in the section between the excitation position and the tips demonstrates a strong lateral confinement of the FL.

Self-assembled organic structures are highly flexible because constituent molecules are held together by noncovalent bonds. This property has been exploited in the development of flexible organic devices such as displays, transistors, and lasers.[28,29] Similarly, TC nanofibers are highly flexible;[30] therefore, those on a solid substrate can be transformed into various shapes by micromanipulation.[31] Panels e and f in Figure 1 show an optical micrograph and FL microscopy image, respectively, of the nanofiber identical to that shown in Figure 1b−d after being bent into an "S" shape with radii of curvature of ∼5 μm. The FL microscopy image obtained by exciting the position near the tip of the nanofiber showed the spot at the other tip, indicating that the FL passed through even the sharply bent fiber (Figure 1g). The low bending loss property together with high flexibility of TC nanofibers makes them as promising building blocks in miniaturized photonic circuit devices. Our detailed investigation on the active waveguiding in TC nanofibers revealed that the low bending loss property is attributed to the exciton polariton (EP) effect.[32] The FL generated by the optical excitation strongly couples with molecular excitons and propagates in the form of the EPs. The EP effect results in a substantially large refractive index of a nanofiber, thereby resulting in a large difference between the refractive index of the nanofiber and that of the surrounding media and leading to

Received: March 29, 2013
Accepted: June 14, 2013
Published: June 26, 2013

   dx.doi.org/10.1021/am4011379 | *ACS Appl. Mater. Interfaces* 2013, 5, 6182−6188

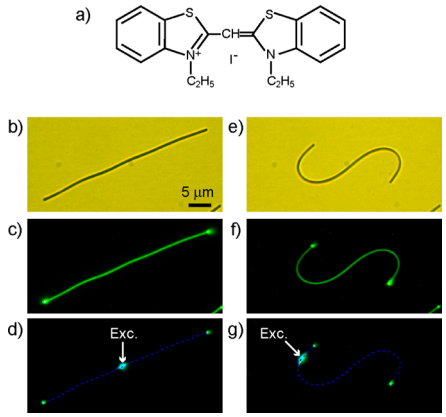

Figure 1. (a) Molecular structure of TC. (b) Optical micrograph and (c) FL microscopy image of a nanofiber on the glass substrate. The excitation and detection wavelength in the FL microscopy imaging were $\lambda < 475$ nm and $\lambda > 510$ nm, respectively. (d) FL microscopy image of the nanofiber recorded by exciting the position labeled "Exc." with a focused laser beam ($\lambda = 405$ nm). Dashed line representing the nanofiber is an eye guide. (e) Optical micrograph and (f) FL microscopy image of the nanofiber bent into an "S" shape by micromanipulation. (g) FL microscopy image of the bent nanofiber recorded by exciting the position labeled "Exc.".

the strong lateral confinement as well as the low bending loss property.

In this study, we investigate the mechanical flexibility and bending loss properties of TC nanofibers and explore the possibility of their application to miniaturized photonic circuit devices. In section 3.1, we report the fabrication of microring resonators by micromanipulation of TC nanofibers. Microring resonators are ideally suited to study the flexibility and bending loss properties because the flexibility determines the minimum ring size and the bending loss property affects the resonator performance. Moreover, the ring resonators that confine the EPs are attractive from the viewpoints of both device applications and fundamental science because they can be used in photonic devices as described in section 3.2, and they can be novel systems to study the strong light−matter interactions. In a previous study, we reported our initial attempt at micromanipulation of TC nanofibers for photonic device fabrication.[31] Subsequently, we have refined our micromanipulation techniques to enable the fabrication of smaller and more complex structures. Here, we show that the rings with a radius as small as 1.6 μm can be fabricated and can function as ring resonators. In section 3.2., we describe the application of the microring resonators to miniaturized photonic circuit devices. We fabricate ring resonator channel add/drop filters comprising of a microring and nanofibers that function as I/O bus channels. The devices exhibit high performance, given their micrometer-scale dimensions.

2. EXPERIMENTAL SECTION

2.1. Sample Preparation. TC was purchased from Hayashibara Corp. and used without further purification. TC dissolved in hot water (≳40 °C) self-assembles into nanofibers with a length of up to ∼250 μm as the solution is cooled to room temperature. The nanofibers have a rectangular cross -section with smooth surfaces with nanometer-scale roughness, which lead to low scattering loss in the FL propagation.[10] A typical height of the nanofibers is 100−200 nm and their width can be controlled from ∼100 nm to ∼1 μm by varying the solution temperature and/or cooling speed. High solution temperature and rapid cooling result in the formation of narrower nanofibers. In the present study, we prepared a TC solution (∼0.1

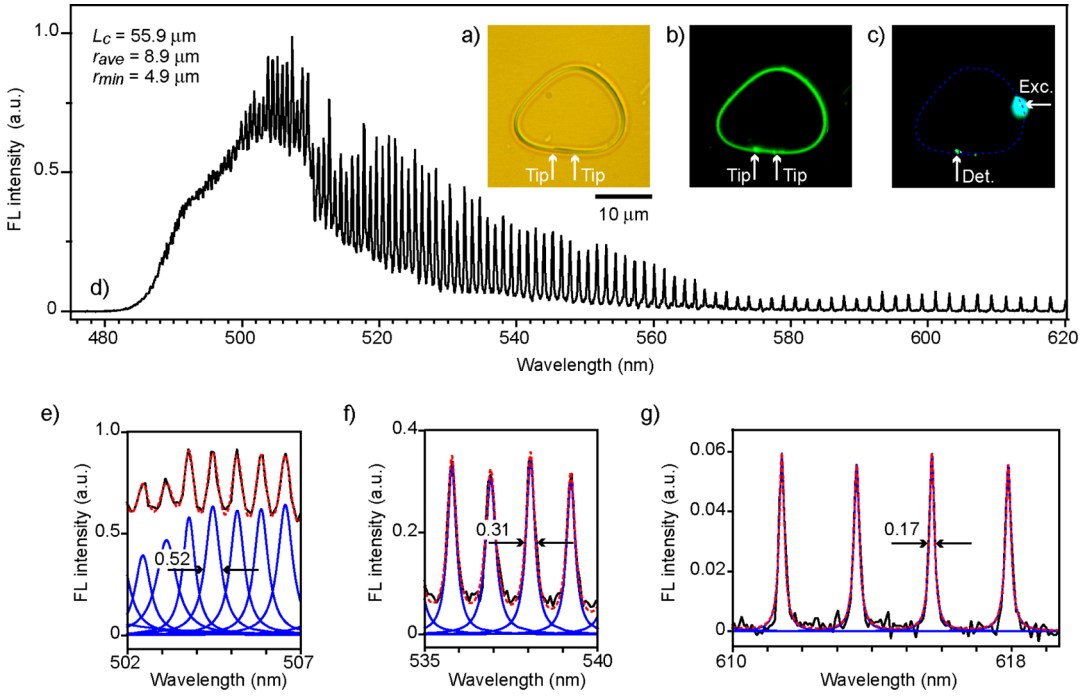

Figure 2. (a) Optical micrograph and (b) FL microscopy image of a microring with $r_{ave} = 8.9$ μm. White arrows indicate the positions of both the fiber tips. (c) FL microscopy image of the ring recorded by exciting the position labeled "Exc." by a focused laser beam. Dashed line representing the ring is an eye guide. (d) Spatially resolved FL spectrum recorded by exciting the position labeled "Exc." and detecting the FL at "Det." (e−g) Comparison between the observed and fitted spectra. Black curves, observed spectrum; blue curves, Lorentzian peaks; and red dashed curves, fitted spectrum.

dx.doi.org/10.1021/am4011379 | ACS Appl. Mater. Interfaces 2013, 5, 6182−6188

mM) at 60 °C and cooled it to room temperature in ambient conditions. The width of the resulting nanofibers, used to construct the devices in this work, was distributed around d = 200 nm. The solution containing the nanofibers was drop-casted onto a glass substrate (microscope cover glass, 22 mm × 22 mm) coated with a thin oil layer ($n \approx 1.48$) of a few tens of nanometers thickness,[33] and the solvent was allowed to evaporate. The thin oil layer prevents the nanofibers from adhering to the glass surface, rendering them significantly easier to manipulate.

2.2. Micromanipulation. Micromanipulation was performed using a glass probe tip (tip diameter ≈ 200 nm) attached to a piezo-micromanipulator (Kleindiek). The sample was placed on the motorized stage (Prior, H-101) of an optical microscope (Olympus, BX-51). The nanofibers were manipulated by moving both the glass tip and the sample under microscope observation using a long-working-distance objective lens (50× or 100×).[33]

2.3. FL Microscopy Imaging and Spatially Resolved FL Microscopy by Focused Laser Beam Excitation. The output of a continuous wave diode laser (Coherent, Radius405, λ = 405 nm) was coupled to an epi-illumination FL microscope (Olympus, BX-51). The laser beam was focused onto the sample with a 100× objective lens (NA = 0.95, spot size ≈ 300 nm). The FL from the sample was collected by the same objective lens and recorded by a color CCD camera (Jenoptic, ProgRes C10) through a long-pass filter that blocks the excitation laser. In spatially resolved FL microscopy, the FL was imaged onto the entrance slits of an imaging monochromator (Acton Research, SpectraPro 2150). The FL passed through the slits was recorded by a liquid-nitrogen-cooled back-illuminated CCD camera (Princeton Instruments, Spec10, 1340 pixel ×400 pixel). The captured image was spectrally and spatially resolved along the horizontal and vertical axes of the CCD camera, respectively. The FL spectrum was obtained by extracting a horizontal cross section of the image.

3. RESULTS AND DISCUSSION

3.1. Microring Resonators. When two TC nanofibers contact each other with a certain contact length, EPs transfer from one nanofiber to the other through evanescent coupling.[31,33] Therefore, a ring structure constructed by jointing both ends of a nanofiber can function as a ring resonator. The performance of a ring resonator, i.e., the finesse and Q-factor, is governed by losses in the resonator. These losses can be divided into the following components: the intrinsic propagation loss and the extrinsic losses that include the bending loss and the transmission loss in the contact region of both fiber ends. Thus, if we fabricate rings of different radii and constant transmission loss, we can extract information on the propagation and bending losses by comparing the finesses and Q-factors of the rings.

First, we fabricated a relatively large ring in which the bending loss is expected to be negligible. Bending loss was later assessed by comparing the performances of the large ring with those of small rings. Figures 2a and b show an optical micrograph and FL microscopy image, respectively, of a ring with a circumference of L_c = 55.9 μm and average radius $r_{ave} = L_c/2\pi$ = 8.9 μm. The radius of the curvature of the most tightly bent part of this ring is r_{min} = 4.9 μm. Both ends of the nanofiber were jointed with a contact length of l = 4.8 μm. The connection is rather robust probably because of the intermolecular forces. The FL microscopy image recorded by exciting the ring with a focused laser beam showed weak FL spots at the positions of both fiber tips (Figure 2c). We recorded the spectrum of one of the spots by spatially resolved FL microscopy (Figure 2d).[27,31−33] Sharp peaks were observed over a wide spectral range (490−620 nm). The spectrum could be well fitted by a superposition of Lorentz functions, as shown in Figure 2e−g. The peak widths $\Delta\lambda$ evaluated from the full width at half-maximum of individual Lorentzian peaks were ∼0.5 nm for $\lambda \approx$ 500 nm, and decreased with increasing λ. At $\lambda \approx$ 615 nm, $\Delta\lambda$ was ∼0.17 nm and was comparable to the spectral resolution of our setup.

To confirm that these peaks are attributed to the ring resonator modes, we evaluated the group index (n_g) of the nanofiber from the observed peak positions. For a ring resonator, n_g is related to the spacing between peaks (free spectral range, FSR) as follows: $n_g = \lambda^2/(\mathrm{FSR}L_c)$. Using this equation and FSR measured from the spectrum, n_g was calculated and plotted in Figure 3a with that evaluated in our previous study.[32] The n_g values obtained in this study agree well with those of the previous study and show a divergent increase with a decrease in λ, which is a characteristic feature of n_g in the energy region of the lower blanch EPs.[32] This result confirms that the observed peaks are attributed to the ring resonator modes.

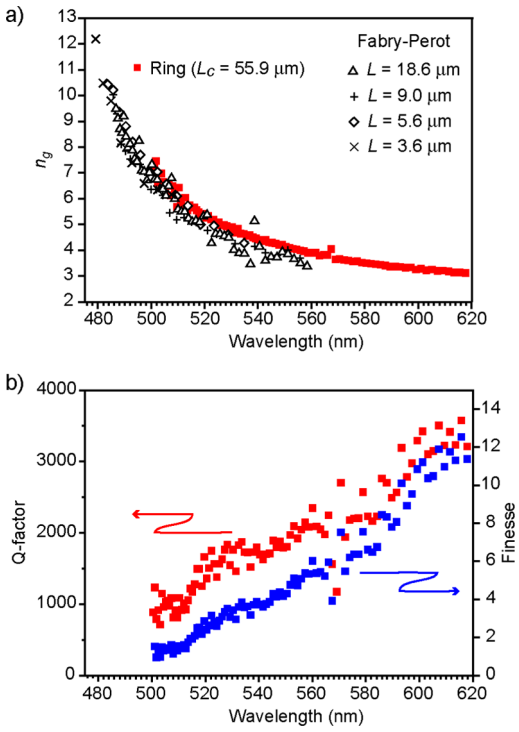

Figure 3. (a) Plot of n_g evaluated from the FL spectrum of the ring with r_{ave} = 8.9 μm (red squares). Symbols show n_g evaluated from the observed Fabry−Perot modes for nanofibers of different lengths (L = 3.6−18.6 μm).[32] (b) Plots of Q-factor (red squares) and finesse (blue squares).

To evaluate the performance of the ring resonator, we calculated the finesse (F) and Q-factor (Q) using the relationships $F = \mathrm{FSR}/\Delta\lambda$ and $Q \approx \lambda_0/\Delta\lambda$, where λ_0 is the peak wavelength. These quantities are plotted in Figure 3b as functions of λ. Both F and Q increase monotonically with λ, attaining values of ∼12 and ∼3500, respectively, in the long-wavelength region. These trends can be understood by considering wavelength dependence of the propagation loss. In the short-wavelength region, which is close to the exciton absorption band, EPs have a large exciton character, and therefore, exhibit fast decay through processes such as scattering with acoustic phonons.[30] Thus, the propagation loss in this wavelength region is large, resulting in low F and Q values. As λ increases, a light character dominates in the EPs

dx.doi.org/10.1021/am4011379 | ACS Appl. Mater. Interfaces 2013, 5, 6182−6188

and their decay is suppressed.[32] This leads to a low propagation loss, resulting in high F and Q values.

In contrast to the propagation loss, the bending loss should increase with λ because the refractive index of a nanofiber decreases with λ.[32] However, the Q and F values increase monotonously with λ (Figure 3b). This fact is consistent with our assumption that the bending loss in this ring is negligible because of its relatively large size.

By careful micromanipulation, we succeeded in constructing smaller rings with r_{ave} as small as 1.6 μm. The insets of Figures 4a–d show the optical micrographs and FL microscopy images

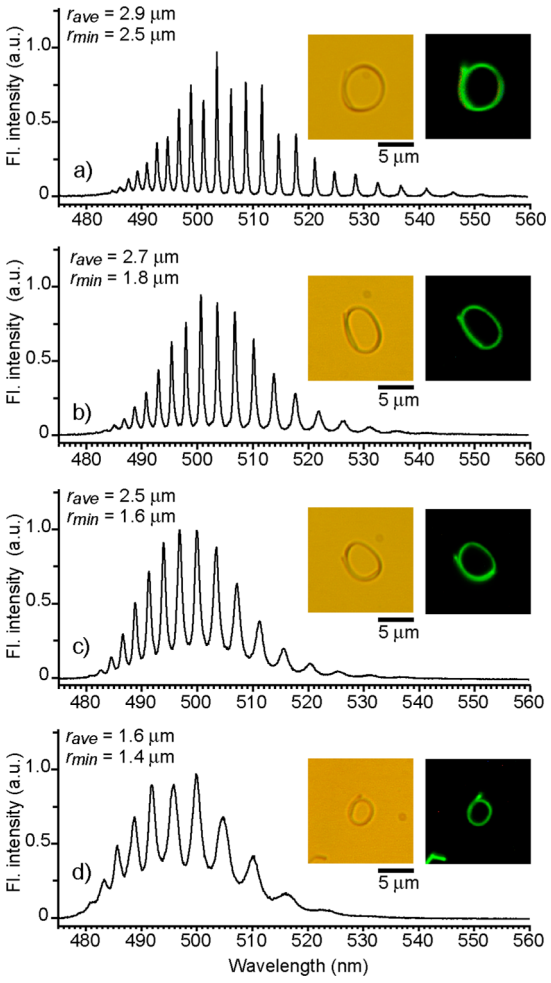

Figure 4. Spatially resolved FL spectra of different-sized rings; r_{ave} = (a) 2.9, (b) 2.7, (c) 2.5, and (d) 1.6 μm. The insets show optical micrographs and FL microscopy images of the rings.

of the fabricated rings (r_{ave} = 2.9, 2.7, 2.5, and 1.6 μm; r_{min} = 2.5, 1.8, 1.6, 1.4 μm). Throughout the fabrication process, particular attention was given to the contact length of both the nanofiber end regions (l). Because l influences the transmission loss along the contact regions, it affects the resonator performance. To clarify the effect of the propagation and bending losses on the resonator performance, the transmission loss in these rings must be constant. Therefore, we made l to a nearly uniform length of 4–6 μm, which is close to that of the large ring shown in Figure 2. The rings were excited by the focused laser beam and the spectra of the FL spots at the fiber tip positions were measured. All of the spectra showed clear resonance peaks, whose spacing increases with decreasing ring size, proving that the rings functioned as ring resonators (Figure 4a–d). Note that even the smallest ring with r_{ave} = 1.6 μm (r_{min} = 1.4 μm) functioned as a ring resonator. Such small ring resonators operating in the visible wavelength region ($\lambda \approx$ 500 nm) have been rarely developed using other waveguide technologies. It also should be noted that although the smallest ring that we could fabricate had r_{ave} = 1.6 μm, TC nanofibers are flexible enough to form yet smaller rings. The minimum r_{ave} was merely limited by the resolution of our micromanipulation system, which is determined by the diffraction limit of light.

The spectra of the small rings clearly show the effect of bending loss on the resonator performance. Bending loss causes weakening and broadening of the resonance peaks in the long-wavelength region of each spectrum. For example, the ring with r_{ave} = 2.9 μm exhibits the maximum intensity peak at $\lambda \approx$ 504 nm, and the peaks become weaker and broader with increasing λ (Figure 4a). As ring radius decreases, the most intense peak shifts toward shorter wavelengths, indicating that bending loss reduces resonator performance in the long-wavelength region. On the other hand, the effect of propagation loss can be seen in the short-wavelength region. For the ring with r_{ave} = 2.9 μm, the resonance peaks were observed for $\lambda >$ ~485 nm (Figure 4a). With decreasing ring size, they appear in the shorter-wavelength region; for the smallest ring, they are observed for $\lambda \gtrsim$ 480 nm (Figure 4d). This extension of the resonance peak region toward shorter wavelengths is attributed to large propagation loss in the short-wavelength region. Because of large propagation loss, a round trip of the EPs, which yields the resonance peaks, is possible only in small rings. Therefore, as the ring size decreases, the visibility of the resonance peaks in the shorter-wavelength region increases.

The spectra were best-fitted by a superposition of Lorentz functions and $\Delta\lambda$ and FSR were evaluated for each ring. In panels a and b in Figure 5, F and Q of the small rings as functions of wavelengths are plotted with those of the large ring shown in Figure 3 (r_{ave} = 8.9 μm) in which the bending loss is negligible. These curves well demonstrate the λ- and r_{ave}-dependence of the resonator performance, which were qualitatively discussed in the previous paragraph. The F and Q values of the small rings form convex curves with a well-defined peak that shifts toward shorter wavelengths as r_{ave} decreases, whereas those of the large ring monotonically increase with λ. This is because of the reduction in the resonator performances due to the bending loss in the long-wavelength region. On the other hand, in the short-wavelength region ($\lambda \lesssim$ 490 nm), the F values of all small rings almost overlap with each other, implying that only the propagation loss and the transmission loss along the contact regions, which are constant for all the rings, determine the F values and the bending loss is negligible in this wavelength region. From the peak values of the Q (F) curves, we evaluated the highest Q (F) values as $Q \approx$ 1500 (8), 800 (6), 600 (3), and 300 (2) for the rings with r_{ave} = 2.9, 2.7, 2.5, and 1.6 μm, respectively.

3.2. Microring Resonator Channel Drop/Add Filters.

We have demonstrated that the microrings constructed from TC nanofibers function as ring resonators with Q up to ~3500 (F up to ~12). Now, we describe the application of such microring resonators to miniaturized photonic circuit devices. A microring resonator with one or two closely located I/O bus channel waveguides, which inputs (outputs) optical signals to (from) the ring, is commonly used in photonic circuits as a channel drop/add filter.[34] In addition, the application of microring resonators to sensing devices has recently attracted

dx.doi.org/10.1021/am4011379 | ACS Appl. Mater. Interfaces 2013, 5, 6182–6188

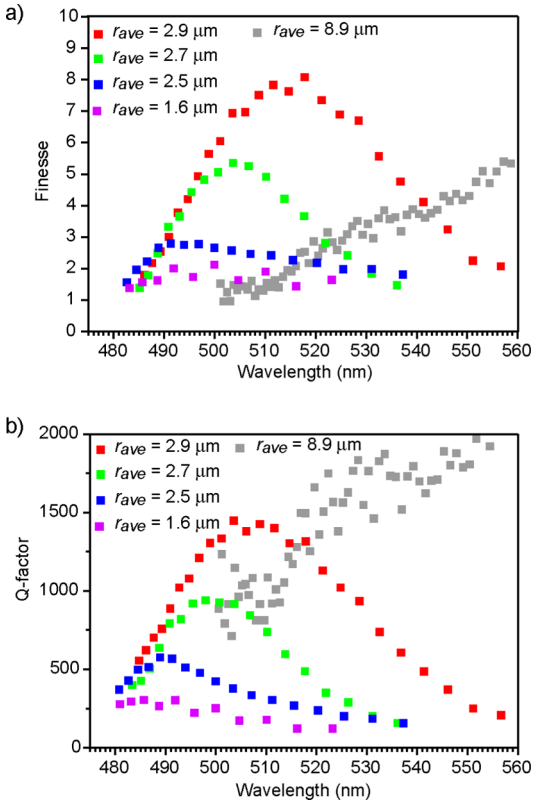

Figure 5. Plots of the (a) finesses and (b) the *Q*-factors of the rings with r_{ave} = 1.6–8.9 μm.

considerable attention.[35,36] Therefore, the fabrication of such devices at a miniaturized scale using TC nanofibers is of particular interest. First, we fabricated a channel drop filter that consists of a microring and a single I/O bus channel fiber. When the I/O bus channel nanofiber and the microring are placed close enough to allow evanescent coupling, the EPs propagating along the bus fiber can be transferred to the ring. In this situation, the EPs that resonate in the ring destructively interfere with those in the bus fiber passing through the coupling region. Consequently, the EPs that transmit through the coupling region should exhibit a drop in the intensity (the drop channel) at the wavelengths of the ring resonator modes.

Figures 6a and b show the optical micrograph and FL microscopy images, respectively, of a microring with r_{ave} = 3.9 μm (r_{min} = 2.2 μm) and a straight nanofiber with a length of 26.5 μm, which is to be used as the I/O bus channel fiber. Prior to assembling these elements, we investigated the waveguiding properties of the I/O bus channel nanofiber. We later use these data to normalize the spectrum of the fabricated device. We excited the position near the left tip of the nanofiber by a focused laser beam and recorded the spectrum of the FL spot at the right tip of the nanofiber (labeled "Out" in the insets of Figure 6c). The spectrum obtained shows a broad FL ranging from ~485 to ~560 nm with a rapid intensity oscillation, which is attributed to the Fabry–Perot modes due to reflection of the EPs at both end faces of the nanofiber.[32]

We moved the I/O bus channel nanofiber toward the ring by micromanipulation to enable evanescent coupling between the structures. When the nanofiber contacted the ring perimeter, the spectrum measured at "Out" showed a series of dips. For a ring resonator channel drop filter, an optimum structure that

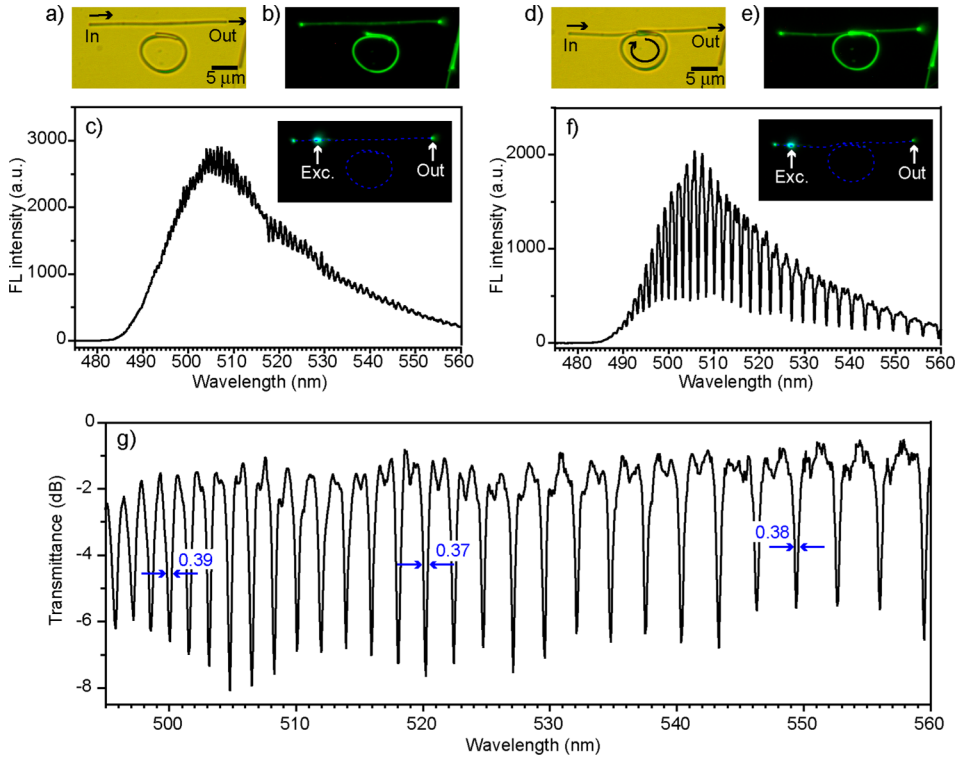

Figure 6. (a) Optical micrograph and (b) FL microscopy image of the microring (r_{ave} = 3.9 μm) and the straight nanofiber. c) Spatially resolved FL spectrum recorded by exciting the position labeled "Exc." and detecting FL at the position labeled "Out" (see the inset). Dashed lines representing the nanofibers are eye guides. Optical micrograph (d) and FL microscopy image of the channel drop filter. (f) Spatially resolved FL spectrum recorded by exciting the position labeled "Exc." and detecting FL at "Out" (see the inset). (g) Transmittance spectrum of the device.

dx.doi.org/10.1021/am4011379 | ACS Appl. Mater. Interfaces 2013, 5, 6182–6188

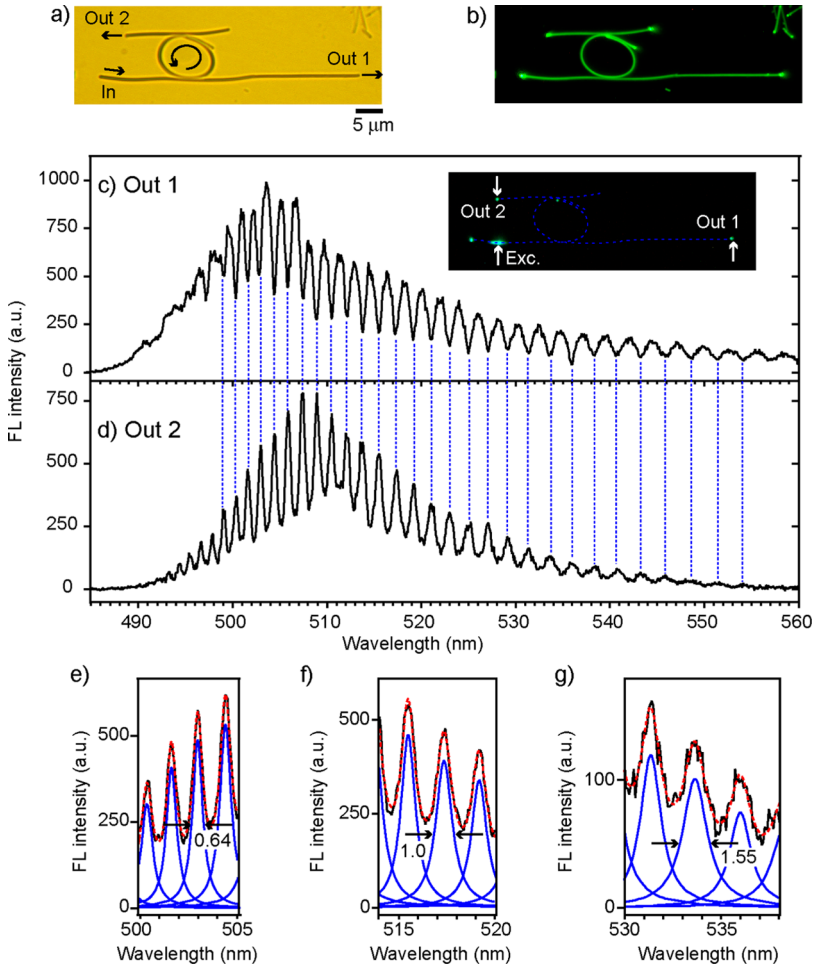

Figure 7. (a) Optical micrograph and (b) FL microscopy image of the channel add filter. (c) Spatially resolved FL spectrum recorded by exciting the position labeled "Exc." and detecting FL at "Out 1" (see the inset). Dashed lines representing nanofibers are eye guides. (d) Spatially resolved FL spectrum recorded by detecting FL at "Out 2". Vertical blue dashed lines connect the dip positions in c with the peak positions in d to highlight their agreement. (e–g) Comparisons between the observed spectrum in d and the fitted spectrum. Black curves, observed spectrum; blue curves, Lorentzian peaks; and red dashed curves, fitted spectrum.

provides the highest extinction ratio at the drop channels has been studied in detail.[37,38] To obtain the highest extinction ratio, the power splitting ratio between the light (EP) being loaded into the ring and that passing through the coupling region must be optimized with respect to the finesse of the ring resonator.[39] In our device, the power splitting ratio can be tuned by varying the contact length between the ring and I/O bus fiber to yield the highest extinction ratio. It was observed that the channel widths as well as the extinction ratio sensitively changed with the contact length. High extinction ratios and narrow channel widths were obtained for the contact length of 6.0 μm (Figure 6d, e), the spectrum of which is shown in Figure 6f. To obtain the transmittance spectrum, we normalized this spectrum with respect to that shown in Figure 6c, measured prior to ring contact. The normalized spectrum converted to decibels (dB) is displayed in Figure 6g. From the transmittance spectrum, we observe that extinction ratios at the drop channels are 4–6 dB and the channel widths evaluated by best-fitting the spectrum to Lorentz functions are <0.4 nm over a wide spectral range (490–560 nm). These performances are considerably high for a compact device of micrometer-scale dimensions.

Next, we fabricated a channel add filter by attaching two I/O bus channel fibers to a microring. Figures 7a and b show the optical micrograph and FL microscopy images, respectively, of the fabricated device. The filter comprises a microring with r_{ave} = 4.3 μm (r_{min} = 2.5 μm) and two I/O bus channel nanofibers with lengths of 19.1 and 47.7 μm, which were attached to the upper and lower sections of the ring, respectively. The contact lengths for the upper and lower coupling regions were 2 and 4 μm, respectively. The inset of Figure 7c shows a FL microscopy image of the device recorded by exciting the position near the left tip of the lower nanofiber by the focused laser beam. The FL spots were observed at both the fiber tips, labeled "Out 1" and "Out 2". We measured the spectrum of the both spots by spatially resolved FL microscopy. The spectrum at "Out 1" shows a series of dips, exhibiting the channel drop filter behavior (Figure 7c). The extinction ratios of the drop channels were 2–3 dB. On the other hand, the spectrum measured at "Out 2" shows peaks at the same positions as those of the drop channels (Figure 7d), revealing that the device functions as a channel add filter. In this device, a portion of the EPs that constructively resonate within the ring is coupled to the upper straight nanofiber, and is output at "Out 2". The spectrum measured at "Out 2" was best-fitted by a superposition of Lorentz functions (Figures 7e–g). The widths of the add channels were $\Delta\lambda \approx 0.64$ nm at $\lambda \approx 500$ nm and steadily increased with λ, reaching ~1.55 nm at $\lambda \approx 530$ nm. Similar to

dx.doi.org/10.1021/am4011379 | ACS Appl. Mater. Interfaces 2013, 5, 6182–6188

the single I/O bus channel device, the channel add filter performance is maximized by balancing the finesse of the ring resonator and the power splitting ratios at the two coupling regions.[37,38] Because we could not entirely optimize the splitting ratios for both the contact region in this device, the device performance was suboptimal. Nevertheless, the performance is considerably high for its compact device size. Therefore, our results highlight the remarkable potential of TC nanofibers as building blocks in miniaturized photonic circuit devices.

4. CONCLUSIONS

By micromanipulation of TC nanofibers on glass substrates, we fabricated different-sized microring resonators that confine the EPs within the rings. Because of the high flexibility and low bending loss property of the nanofibers, ring resonators as small as r_{ave} = 1.6 μm could be constructed. The performances of the ring resonators were investigated by spatially resolved FL microscopy. The *Q*-factors (Q) and finesses (F) of the fabricated ring resonators (r_{ave} = 1.6−8.9 μm) were evaluated as $Q \approx 300-3500$ and $F \approx 2-12$. On the basis of the dependence of ring size on resonator performances, we revealed the origins of the optical losses in the resonators. Then, we explored the applicability of TC nanofibers to miniaturized photonic circuit devices. To this end, we fabricated a microring channel drop filter comprising a microring with r_{ave} = 3.9 μm and a single I/O bus channel nanofiber. Given the compact size of the device, high extinction ratios (4−6 dB) were observed at the drop channels. We further fabricated a microring channel add filter comprising a microring with r_{ave} = 4.3 μm and two I/O bus channel nanofibers.

AUTHOR INFORMATION

Corresponding Author

*E-mail: takazawa.ken@nims.go.jp.

Notes

The authors declare no competing financial interest.

ACKNOWLEDGMENTS

We thank Drs. T. Takamasu and K. Sakoda for helpful discussions. This work was supported by the Grant-in-Aid for Scientific Research (24540332), Japan Society for the Promotion of Science.

REFERENCES

(1) Hunsperger, R. G. *Integrated Optics: Theory and Technology*, 5th ed.; Springer: Berlin, 2002.
(2) Mekis, A.; Chen, J. C.; Kurland, I.; Fan, S. H.; Villeneuve, P. R.; Joannopoulos, J. D. *Phys. Rev. Lett.* **1996**, *77*, 3787−3790.
(3) Noda, S.; Tomoda, K.; Yamamoto, N.; Chutinan, A. *Science* **2000**, *289*, 604−606.
(4) Maier, S. A.; Kik, P. G.; Atwater, H. A.; Harel, E.; Koel, B. E.; Requicha, A. A. G. *Nat. Mater.* **2003**, *2*, 229−232.
(5) Bozhevolnyi, S. I.; Volkov, V. S.; Devaux, E.; Laluet, J. Y.; Ebbesen, T. W. *Nature* **2006**, *440*, 508−511.
(6) Lipson, M. *J. Lightwave Technol.* **2005**, *23*, 4222−4238.
(7) Jalali, B.; Fathpour, S. *J. Lightwave Technol.* **2006**, *24*, 4600−4615.
(8) Barrelet, C. J.; Greytak, A. B.; Lieber, C. M. *Nano Lett.* **2004**, *4*, 1981−1985.
(9) Law, M.; Sirbuly, D. J.; Johnson, J. C.; Goldberger, J.; Saykally, R. J.; Yang, P. D. *Science* **2004**, *305*, 1269−1273.
(10) Takazawa, K.; Kitahama, Y.; Kimura, Y.; Kido, G. *Nano Lett.* **2005**, *5*, 1293−1296.
(11) Zhao, Y. S.; Fu, H. B.; Peng, A. D.; Ma, Y.; Xiao, D. B.; Yao, J. N. *Adv. Mater.* **2008**, *20*, 2859−2876.
(12) Zhao, Y. S.; Peng, A. D.; Fu, H. B.; Ma, Y.; Yao, J. N. *Adv. Mater.* **2008**, *20*, 1661−1665.
(13) Zhao, Y. S.; Fu, H. B.; Peng, A. D.; Ma, Y.; Liao, Q.; Yao, J. N. *Acc. Chem. Res.* **2010**, *43*, 409−418.
(14) Kim, F. S.; Ren, G. Q.; Jenekhe, S. A. *Chem. Mater.* **2011**, *23*, 682−732.
(15) Zhao, Y. S.; Xu, J. J.; Peng, A. D.; Fu, H. B.; Ma, Y.; Jiang, L.; Yao, J. N. *Angew. Chem., Int. Ed.* **2008**, *47*, 7301−7305.
(16) Schiek, M.; Balzer, F.; Al-Shamery, K.; Brewer, J. R.; Lutzen, A.; Rubahn, H. −G. *Small* **2008**, *4*, 176−181.
(17) Bao, Q. L.; Goh, B. M.; Yan, B.; Yu, T.; Shen, Z. A.; Loh, K. P. *Adv. Mater.* **2010**, *22*, 3661−3666.
(18) Zhang, C.; Zou, C. L.; Yan, Y. L.; Hao, R.; Sun, F. W.; Han, Z. F.; Zhao, Y. S.; Yao, J. N. *J. Am. Chem. Soc.* **2011**, *133*, 7276−7279.
(19) Zhang, C.; Zhao, Y. S.; Yao, J. N. *Phys. Chem. Chem. Phys.* **2011**, *13*, 9060−9073.
(20) Cui, Q. H.; Zhao, Y. S.; Yao, J. N. *J. Mater. Chem.* **2012**, *22*, 4136−4140.
(21) Balzer, F.; Bordo, V. G.; Simonsen, A. C.; Rubahn, H.-G. *Appl. Phys. Lett.* **2003**, *82*, 10−12.
(22) Balzer, F.; Bordo, V. G.; Simonsen, A. C.; Rubahn, H.-G. *Phys. Rev. B* **2003**, *67*, 115408.
(23) Cheng, C. W.; Luo, Y. *Micro Nano Lett.* **2012**, *7*, 397−401.
(24) Chandrasekhar, N.; Chandrasekar, R. *Angew. Chem., Int. Ed.* **2012**, *51*, 3556−3561.
(25) Chandrasekhar, N.; Mohiddon, M. A.; Chandrasekar, R. *Adv. Opt. Mater.* **2013**, *1*, 305−311.
(26) Hui, P.; Chandrasekar, R. *Adv. Mater.* DOI: 10.1002/adma.201300540.
(27) Takazawa, K. *J. Phys. Chem. C.* **2007**, *111*, 8671−8676.
(28) Forrest, S. R. *Nature* **2004**, *428*, 911−918.
(29) Clark, J.; Lanzani, G. *Nat. Photonics* **2010**, *4*, 438−446.
(30) Takazawa, K. *Chem. Phys. Lett.* **2008**, *452*, 168−172.
(31) Takazawa, K.; Inoue, J.; Mitsuishi, K.; Takamasu, T. *Adv. Mater.* **2011**, *23*, 3659−3663.
(32) Takazawa, K.; Inoue, J.; Mitsuishi, K.; Takamasu, T. *Phys. Rev. Lett.* **2010**, *105*, 067401.
(33) Takazawa, K.; Inoue, J.; Mitsuishi, K.; Kuroda, T. *Adv. Funct. Mater.* **2013**, *23*, 839−845.
(34) Little, B. E.; Chu, S. T.; Haus, H. A.; Foresi, J.; Laine, J. P. *J. Lightwave Technol.* **1997**, *15*, 998−1005.
(35) Ksendzov, A.; Lin, Y. *Opt. Lett.* **2005**, *30*, 3344−3346.
(36) White, I. M.; Oveys, H.; Fan, X. D. *Opt. Lett.* **2006**, *31*, 1319−1321.
(37) Yariv, A. *Electron. Lett.* **2000**, *36*, 321−322.
(38) Yariv, A. *IEEE. Photonics Technol. Lett* **2002**, *14*, 483−485.
(39) To express the power splitting at the coupling region, the transmission coefficient t and the coupling coefficient k, both of which are complex, are introduced. They are normalized as $|t|^2 + |k|^2 = 1$. When a ring has the round-trip attenuation coefficient α, which is related to the finesse of the ring through the relation $F = \pi\alpha^{1/2}/(1 - \alpha)$, the condition yielding the highest extinction ratio is given by $\alpha = |t|$. For details, see refs 37 and 38.